Transactions of the 15th International Conference on
Structural Mechanics in Reactor Technology (SMiRT-15)
Seoul, Korea, August 15-20, 1999 G08/2

A Parametric Study on the Fracture Mechanics Analyses of Through-Wall and Surface Cracked Pipe

Hyun-Su Kim, Yoon-Suk Chang and Tae-Eun Jin

Korea Power Engineering Company, Korea

ABSTRACT : In the last decades, a number of experiments and numerical analyses had been performed, in conjunction with the development of simplified analytical methods to verify the fracture behavior of cracked nuclear piping. However, the necessity of further investigation for the analytical methods was issued because of the discrepancies with the experimental data. The objective of this paper is to find out the optimum method. To do this, numerous analytical and finite element analyses were carried out for various pipe and crack geometries, and the results were compared with the corresponding experimental data.

1. INTRODUCTION

Since 1980's, elastic plastic fracture mechanics(EPFM) technology in nuclear piping has been enhanced through several international research programs[1~4]. The emphasis on these programs was the development of experimental data and analytical methods to verify fracture behavior of the cracked piping, and thereafter considerable products were achieved. During the development stage of these programs, analytical methods and finite element method(FEM) were utilized. However, it was issued that further investigation for the analytical methods was necessary because discrepancies with the corresponding experimental data were observed in some cases. In this paper, therefore, numerous analytical analyses and FE analyses were carried out for various pipe and crack geometries to find out the optimum method.

2. FRACTURE MECHANICS ANALYSIS

To verify the validity of the analytical methods developed previously[1~6], a number of analytical analyses and FE analyses were performed for circumferentially through-wall and surface cracked pipes under bending load. Fig. 1 shows the schematic of the circumferentially through-wall cracked pipe and Fig. 2 shows the circumferentially surface cracked pipe under bending. Representative characteristics of the analytical methods are summarized in Table 1, and the pipe and crack geometries from the quasi-static experimental data[1,2] at 288°C are summarized in Table 2 and Table 3, respectively.

2.1 Through-Wall Cracked Pipe

Analytical analyses were performed using NRCPIPE code[7] for both the base models which experimental data[1,2] were available and specific models in which R_m/t, Ramberg-Osgood parameters were varied. In these analyses, GE/EPRI, Paris/Tada, LBB.NRC, LBB.BCL1, LBB.BCL2, LBB.ENG2, NSC(Net Section Collapse), ASME IWB methods were used, and crack initiation and maximum moment were determined by using the values corresponding to the J_{IC} and $(dJ/da)_{app}=(dJ/da)_{mat}$, respectively.

EPFM analyses were also performed using ABAQUS code for both the base models and specific models in same manner with the analytical analyses. Fig. 3 shows the 3-dimensional

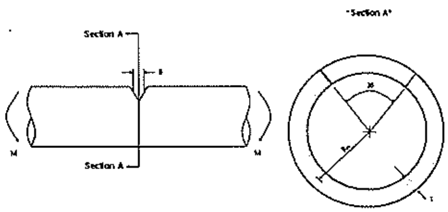

Fig. 1 Schematic of circumferentially through-wall cracked pipe

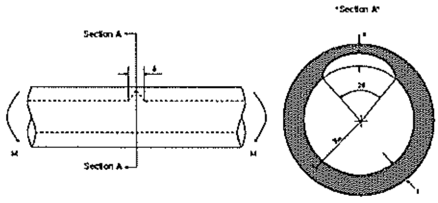

Fig. 2 Schematic of circumferentially surface cracked pipe

Table 1 Characteristics of the analytical methods for cracked pipe[1~6]

Method		Characteristics
Through -Wall Cracked Pipe	GE/EPRI	$J=\pi a[\frac{R_m}{I}]^2\ [F(a/b,R_m/t)]^2\frac{M^2}{E}+\alpha\varepsilon_o\sigma_o c(\frac{a}{b})h_1(a/b,n,R_m/t)[\frac{M}{M_o}]^{n+1}$
	Paris/Tada	$J=E(\pi R_m)[H(\theta)]^2(\phi_e^c)^2+\frac{\sigma_f R_m F_j(\theta)}{M^{rp}(\theta)}\int_0^{\phi_p^c} M(\theta)d\phi_p^c$
	LBB.NRC	$\phi_p^c=\alpha(\frac{\sigma_o}{\sigma_f})^{n-1}\phi_e(\theta_{eff})$
	LBB.BCL1	$\phi_p^c=K'\alpha(\frac{\sigma}{\sigma_f})^{n-1}\phi_e^c(\theta_{eff})$
	LBB.BCL2	$\phi_p^c=(\frac{t}{t_e})^{n-1}(\frac{\pi}{4R})^n\alpha(\frac{\sigma}{\sigma_f})^{n-1}\phi_e^c$
	LBB.ENG2	$J=E(\pi R_m)[H(\theta)]^2(\phi_e^c)^2+\frac{\alpha}{(E\sigma_o^{n-1})}\frac{\pi R_m}{2(n+1)}H_B(n,\theta)L_B(n,\theta)I_b(\theta)[\frac{M}{\pi R_m^2 t}]^{n+1}$
	NSC	$M_{NSC}=2\sigma_f R_m^2 t[2\sin\beta-\sin\theta]$
	ASME IWB	$M=\frac{4I\sigma_f}{\pi D_o}(2\sin\beta-\sin\theta)/Z$
Surface Cracked Pipe	SC.TNP1	$J=\frac{M}{\pi R_m^2 t}F_B(\frac{a}{t},\frac{\theta}{\pi})\sqrt{(\pi a)}+\alpha\sigma_o\varepsilon_o(1-\frac{a}{t})ah_1(\frac{\sqrt{3}t\sigma}{2b\sigma_o})^{n+1}$
	SC.TNP2	$L=(n-1)t$
	SC.TKP1	$J=\frac{M}{\pi R_m^2 t}F_B(\frac{a}{t},\frac{\theta}{\pi})\sqrt{(\pi a)}+\alpha\sigma_o\varepsilon_o(1-\frac{a}{t})ah_1(\frac{k\sigma}{p_o})^{n+1}$
	SC.TKP2	$L=(n+1)/(2n+1)t$
	SC.ENG1	$J=\frac{M}{\pi R_m^2 t}F_B(\frac{a}{t},\frac{\theta}{\pi})\sqrt{(\pi a)}+[\frac{\alpha M^{n+1}}{2t\theta M_o^{n+1}(R_m-t/2+a)(n+1)}][\frac{\pi}{4R}]^n[H(\frac{a}{t})^{n-1}\frac{dG(a/t)}{d(a/t)}$ $+(n-1)G(\frac{a}{t})[H(\frac{a}{t})^{n-2}]\frac{dH(a/t)}{d(a/t)}]$
	SC.ENG2	$H(a/t)=\frac{2}{K(a/t)}$
	NSC	$M_{NSC}=2\sigma_f R_m^2 t[2\sin\beta-\frac{a}{t}\sin\theta]$
	ASME IWB	$M=\frac{4I\sigma_f}{\pi D_o}(2\sin\beta-\frac{a}{t}\sin\theta)/Z$

Table 2 Experimental data for through-wall cracked pipe[1,2]

Item	SA376 TP304		A515 Gr.60 (1)	A515 Gr.60 (2)
	Base Metal	Weld Metal	Base Metal	Base Metal
E (GPa) / υ	183 / 0.3	183 / 0.3	179.3 / 0.3	179.3 / 0.3
σ_Y / σ_U (MPa)	139 / 450	325 / 466	230.7 / 543.6	230.7 / 543.6
α / n	9.69 / 3.13	2.28 / 11.03	1.10 / 5.50	1.10 / 5.50
J_{IC} (kN/m)	100		216	216
C / m	164 / 0.703		166 / 0.483	166 / 0.483
$2a/\pi D_m$ (%)	37.1		6.25	37.0
D_{in} / D_{out} (mm)	139.7 / 168.3		665.6 / 711.0	663.8 / 711.0
Thickness (mm) / R_m/t	14.3 / 5.39		22.7 / 15.16	23.6 / 14.56

Table 3 Experimental data for surface cracked pipe [1,2]

Item	SA376 TP304 Base Metal			A106 Gr.B Base Metal	
	SS(1)	SS(2)	SS(3)	CS(1)	CS(2)
E (GPa) / υ	183.1 / 0.3	183.1 / 0.3	182.4 / 0.3	193.4 / 0.3	210.5 / 0.3
σ_Y / σ_U (MPa)	146.9 / 448.9	146.9 / 448.9	138.6 / 449.6	212.4 / 467.5	319.9 / 621.5
α / n	8.66 / 3.37	8.66 / 3.37	11.23 / 3.57	0.50 / 7.22	1.97 / 5.37
J_{IC} (kN/m)	873	873	646	259	108
C / m	0.332 / 0.854	0.332 / 0.854	0.261 / 0.982	0.138 / 0.988	0.117 / 0.814
$2c/\pi D_m$ (%) / a/t	25.0 / 0.50	50.2 / 0.63	51.8 / 0.66	50.8 / 0.63	50.3 / 0.68
D_{in} / D_{out} (mm)	154.1 / 168.3	153.4 / 167.4	141.4 / 168.6	154.4 / 169.3	137.9 / 167.5
Thickness (mm) / R_m/t	7.1 / 11.35	7.0 / 11.46	13.6 / 5.70	7.44 / 10.88	14.8 / 5.16

FE model for the circumferentially through-wall cracked pipe, and only 1/4 of the pipe was modeled because of the geometric symmetry. Crack initiation and maximum moment were determined by using the values corresponding to the J_{IC} and $T_{app}>T_{mat}$, respectively.

2.2 Surface Cracked Pipe

Analytical analyses were performed using NRCPIPES code[8] for both the base models represented in Table 3 and specific models in which R_m/t, $2c/\pi$ D_m, and a/t were varied, and overall analysis procedures used in these analyses were similar to that of the through-wall cracked pipe. SC.TNP1, SC.TNP2, SC.TKP1, SC.TKP2, SC.ENG1, SC.ENG2, NSC, Battelle and Kurihara modified NSC[6,9], ASME IWB methods were used, and crack initiation and maximum moment were determined by using the values corresponding to the J_{IC} and $(dJ/da)_{app}=(dJ/da)_{mat}$, respectively.

EPFM analyses were also performed using ABAQUS code for five base models. Fig. 4 shows the 3-dimensional FE model for the circumferentially surface cracked pipe, and only 1/4 of the pipe was modeled because of the geometric symmetry. Crack initiation and maximum moment were determined by using the values corresponding to the J_{IC} and $T_{app}>T_{mat}$, respectively.

3. ANALYSIS RESULTS

Comparison of the crack initiation and maximum moments predicted from analytical and FE analyses with the corresponding experimental data and the major observations are as follows.

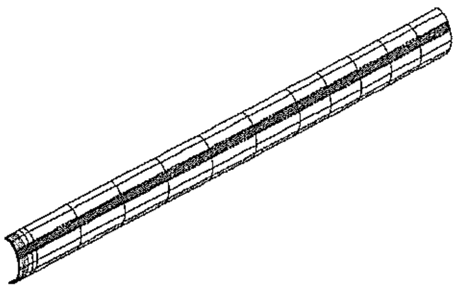

Fig. 3 Finite element model for through-wall cracked pipe

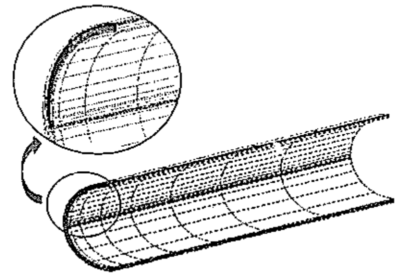

Fig. 4 Finite element model for surface cracked pipe

3.1 Through-Wall Cracked Pipe

Fig. 5 and Fig. 6 show the ratio of the predicted moments obtained by analytical and FE methods to the experimental ones for three cases, one for stainless steel and two for carbon steel, respectively. As shown in these figures, the predicted moments from various methods are lower than experimental moments, and the differences between experimental and predicted crack initiation moments are larger than those of the maximum moments. In addition, predicted results using LBB.NRC, LBB.BCL1, and FE methods are similar to the corresponding values for experiments, while GE/EPRI and LBB.BCL2 methods underpredict the load-carrying capacities. Predicted results for maximum moment using NSC method are higher than the experimental moment, and predicted results using Paris/Tada method scatter according to the analysis condition.

Fig. 7 and Fig. 8 show the predicted moments for the variation of R_m/t of A515 Gr.60 base metal with $2a/\pi D_m$=6.25%. As R_m/t increases, load-carrying capacities tend to decrease and similar results are obtained for other cases. Fig. 9 and Fig. 10 show the predicted moments for the variation of α , Ramberg-Osgood parameter, of A515 Gr.60 base metal with $2a/\pi D_m$=37%. In the cases of GE/EPRI, LBB.BCL2, and LBB.ENG2 methods, load-carrying capacities tend to decrease as α increases. However, in the cases of Paris/Tada, LBB.NRC, and LBB.BCL1 methods, load-carrying capacities are not changed. In addition, predicted results obtained by ASME IWB method for the variation of flow stress are summarized in Table 4, and the predicted results using $3S_m$ are lower than those using other

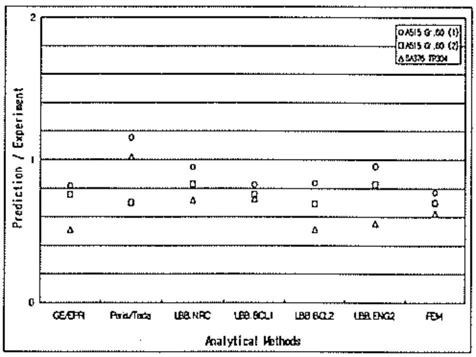

Fig. 5 Crack initiation moment ratio for through-wall cracked pipe

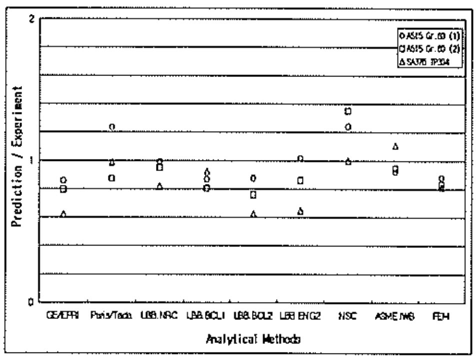

Fig. 6 Maximum moment ratio for through-wall cracked pipe

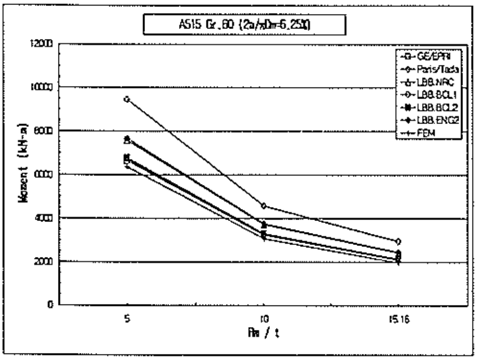

Fig. 7 Predicted initiation moment for the variation of R_m/t

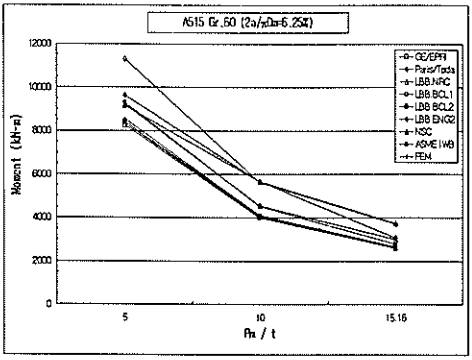

Fig. 8 Predicted maximum moment for the variation of R_m/t

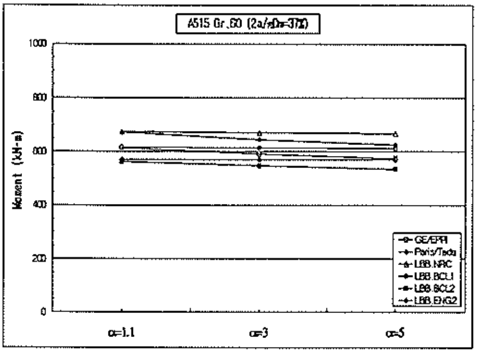

Fig. 9 Predicted initiation moment for the variation of α

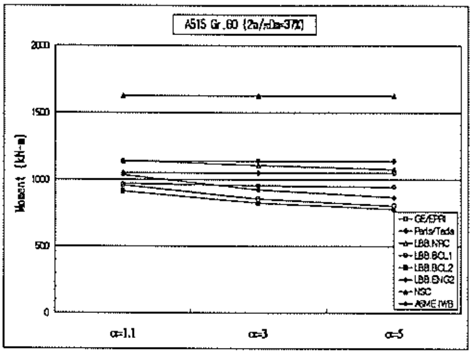

Fig. 10 Predicted maximum moment for the variation of α

Table 4 Predicted maximum moment using ASME IWB method for various flow stress

$2a/\pi D_m$	R_m/t	$M_{Exp.}$ (kN-m)	$M_{Predicted}$ (kN-m)		
			$(\sigma_Y+\sigma_U)/2$	$1.15(\sigma_Y+\sigma_U)/2$	$3S_m$
37%	5	-	3991	4296	3329
	10	-	2075	2233	1731
	14.6	1206	1170	1345	1139

values as flow stress.

On average, the differences between predicted moments obtained by analytical methods and experimental ones are about 24% and 16% for initiation and maximum moments, respectively. And for FEM, the differences are about 30% and 16%, respectively. Specifically, load-carrying capacities predicted by LBB.NRC, LBB.BCL1, and FE methods are similar to the experimental results, and have small scatter to the variation of pipe geometry and material property. And the effect of Ramberg-Osgood parameters to the predicted moment is small except for GE/EPRI, LBB.BCL2, and LBB.ENG2 methods.

3.2 Surface Cracked Pipe

Fig. 11 and Fig. 12 show the ratio of the predicted moments obtained by analytical and FE methods to the experimental ones for five cases, three for stainless steel and two for carbon

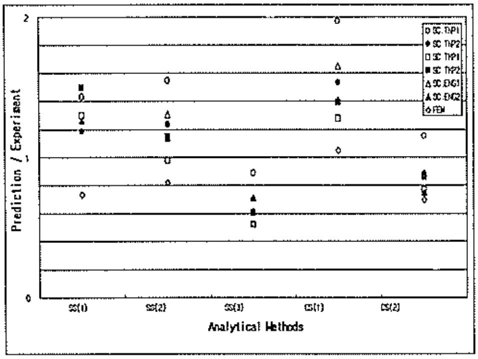

Fig. 11 Crack initiation moment ratio for surface cracked pipe

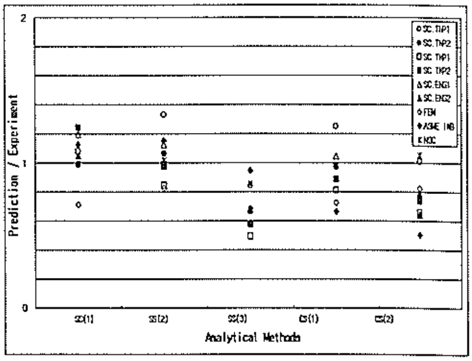

Fig. 12 Maximum moment ratio for surface cracked pipe

steel, respectively. The differences between experimental and predicted maximum moments are smaller than those of the initiation moments. Prediction results using FE method are uniformly underpredictive for given condition. On the contrary, prediction results using analytical methods scatter according to the analysis conditions. In addition, predicted results using SC.TNP2, SC.ENG2, NSC, and FE methods are similar to the corresponding experimental ones. While SC.TNP1 method overpredicts the crack initiation and maximum moments, SC.TKP1 method underpredicts.

Table 5 shows the comparison of original NSC, Battelle and Kurihara modified NSC predicted moments, and Table 6 shows the comparison of predicted moments obtained by original ASME IWB and modified ASME IWB methods using new Z-Factor[10] which was developed in IPIRG-2 program[4]. As shown in Table 5, Battelle modified NSC method is in good agreement with experimental moment for SA376 TP304 stainless steel with small R_m/t, but for other cases, the differences are larger than those of original NSC. Kurihara modified NSC method also tend to underpredict the load-carrying capacities. In Table 6, prediction results using new Z-Factor are in good agreement with experimental moment for A106 Gr.B carbon steel, but for SA376 TP304 stainless steel, prediction results are not in agreement and the differences are rather larger than those of original ASME IWB method which are contrary to what were expected.

Fig. 13 and Fig. 14 show the prediction results for the variation of $2c/\pi\ D_m$ for A106 Gr.B base metal. As $2c/\pi\ D_m$ increases from 25% to 50%, load-carrying capacities tend to decrease and similar results are obtained for other cases. Fig. 15 and Fig. 16 show the prediction results for the variation of R_m/t for A106 Gr.B base metal. As R_m/t increases from 5.2 to 10.8, load-carrying capacities tend to decrease, and similar results are also obtained for other cases.

On average, predicted initiation and maximum moment using analytical methods have

Table 5 Predicted maximum moment using various NSC methods

Ident.	$M_{Exp.}$ (kN-m)	$M_{Predicted}$ (kN-m)		
		$NSC_{Original}$	$NSC_{Battelle}$	$NSC_{Kurihara}$
SS(1)	44.3	44.2	44.9	38.0
SS(2)	29.5	30.1	31.2	25.2
SS(3)	59.6	51.0	58.5	42.2
CS(1)	38.0	37.1	38.9	31.3
CS(2)	80.1	84.3	97.7	68.0

Table 6 Predicted maximum moment using various ASME IWB methods

Ident.	$M_{Exp.}$ (kN-m)	$ASME_{Original}$		$ASME_{Modified}$	
		Z-Factor	$M_{Predicted}$(kN-m)	Z-Factor	$M_{Predicted}$ (kN-m)
SS(1)	44.3	1	49.9	0.782	63.8
SS(2)	29.5	1	34.0	0.781	43.5
SS(3)	59.6	1	56.3	0.794	71.0
CS(1)	38.0	1.272	25.2	0.938	34.1
CS(2)	80.1	1.252	40.3	0.947	53.2

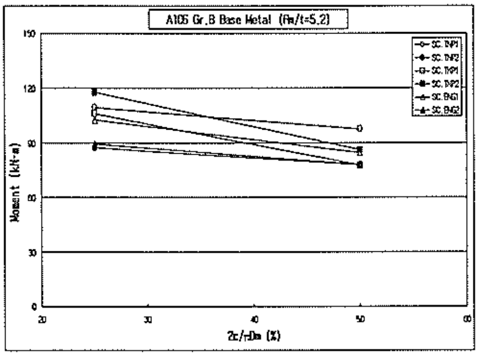

Fig. 13 Initiation moment analysis results for the variation of crack size

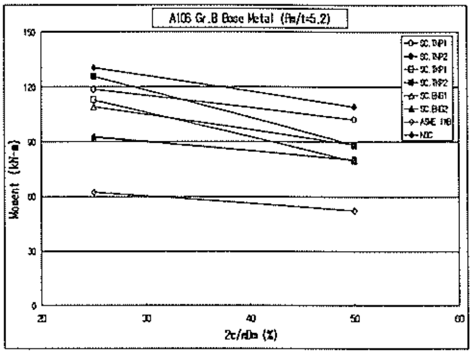

Fig. 14 Maximum moment analysis results for the variation of crack size

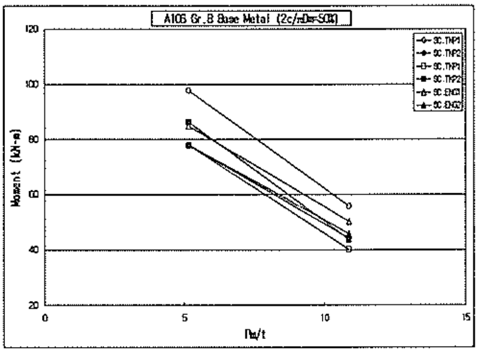

Fig. 15 Initiation moment analysis results for the variation of pipe size

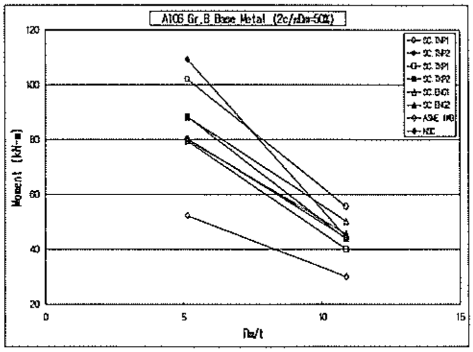

Fig. 16 Maximum moment analysis results for the variation of pipe size

differences of about 30% and 20%, respectively. And for FE method, the differences are about 26% and 25%, respectively. Specifically, load-carrying capacities predicted by SC.TNP2 and SC.ENG2 methods are similar to experimental results, however they have large scatter to the variation of pipe and crack geometry. On the contrary, predicted moments using FE and NSC methods are similar to the experimental results, and they have small variations to the analysis conditions. Battelle modified NSC is in good agreement with experimental moment for certain cases, while for other cases, the differences are rather larger than those of original NSC. Also, Kurihara modified NSC method seems to be underpredictive. Predicted moments using new Z-Factor are in good agreement with the experimental moment for certain case, but for others, the differences are rather large.

4. CONCLUSION

In this paper, to find out optimum analytical method of cracked pipe, a number of numerical analyses and synthetic assessment were performed, and the conclusion of this paper is as follows:

(1) For through-wall cracked pipe, moment prediction results using FE and analytical methods were generally underpredictive.
(2) FE, LBB.NRC and LBB.BCL1 methods seemed to be appropriate methods to predict load-carrying capacity for through-wall cracked pipe.
(3) For surface cracked pipe, moment prediction results using FEM were underpredictive. However, moment prediction results using analytical methods were scattered according to the analysis conditions.
(4) FE and NSC methods seemed to be appropriate methods to predict load-carrying capacity for surface cracked pipe.
(5) Further investigation is necessary for SC.TNP2 and SC.ENG2 methods because the prediction results using these methods scattered according to the analysis conditions, while they were similar to the corresponding values of experiments.

REFERENCES

(1) Wilkowski, G. M., et al., "Degraded Piping Program-Phase II", NUREG/CR-4082, Vol. 1~Vol. 8, 1984.
(2) Wilkowski, G. M., et al., "Short Cracks in Piping and Piping Welds", NUREG/CR-4599, Vol. 1, No. 1~Vol. 4, No. 1, 1994.
(3) Wilkowski, G. M., et al., "International Piping Integrity Research Group Program - Final Report", NUREG/CR-6233, 1991.
(4) Wilkowski, G. M., et al., "International Piping Integrity Research Group(IPIRG-2) Program - Final Report", NUREG/CR-6452, 1996.
(5) Scott, P. M. and Ahmad, J., "Experimental and Analytical Assessment of Circumferentially Surface Cracked Pipes Under Bending", NUREG/CR-4872, 1987.
(6) Wilkowski, G. M., et al., "Fracture Behavior of Short Circumferentially Surface Cracked Pipe", NUREG/CR-6298, 1995.
(7) Battelle, "Through-Wall Crack J-Estimation Scheme Computer Program", NRCPIPE Windows Ver. 3.0, 1996.
(8) Battelle, "Surface Crack J-Estimation Scheme Computer Program", NRCPIPES Windows Ver. 3.0, 1996.
(9) Kurihara, R., Ueda, S. and Sturm, D., "Estimation of the Ductile Unstable Fracture of Pipe with a Circumferential Surface Crack Subjected to Bending", *Nuclear Engineering and Design*, Vol. 106, 1988, pp. 265~273.
(10) Choi, Y. H., Lee, J. B. and Wilkowski, G. M., "Development of New Z-Factors for the Evaluation of a Surface Crack in Nuclear Pipings", *Transactions of the 14th International Conference on SMiRT*, Vol. 4, 1997, pp. 603~610.